



Solid–liquid phase equilibrium diagrams of binary mixtures containing fatty acids, fatty alcohol compounds, and tristearin

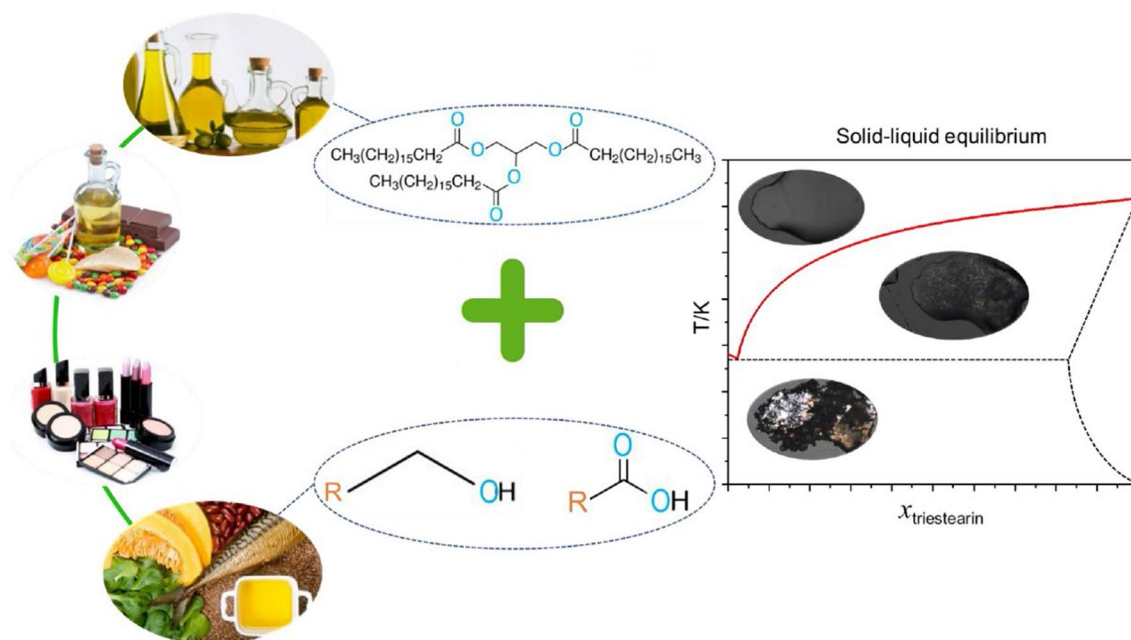
Fernanda Paludetto Pelaquim¹ · Flávio Cardoso de Matos² · Eduardo Augusto Caldas Batista² · Antonio José de Almeida Meirelles² · Mariana Conceição da Costa¹

Received: 9 September 2021 / Revised: 21 January 2022 / Accepted: 27 January 2022 / Published online: 14 March 2022
© The Author(s) under exclusive licence to Associação Brasileira de Engenharia Química 2022

Abstract

Fatty compounds have significant industrial applications as coatings, plastics, cleaning products, emulsifiers, structuring, and gelling agents. Due to these applications, it is important to understand their physical and chemical properties, such as melting behavior, crystallization processes, and phase transitions, all of them related to solid–liquid equilibrium (SLE). In this study, six binary mixtures composed of tristearin (SSS) plus fatty acids (capric acid, lauric acid, and myristic acid) and tristearin plus fatty alcohol compounds (1-decanol, 1-dodecanol, and 1-tetradecanol) were investigated using Differential Scanning Calorimetry (DSC) and optical microscopy analysis. The phase diagrams formed by tristearin + fatty acids presented a monotectic behavior and the phase diagrams formed by tristearin + fatty alcohol compounds, on the other hand, exhibited a solid solution formation on the entire composition range, although the *liquidus* line shape was very similar to that observed in the systems formed by fatty acids. The *liquidus* line of all systems were well-described by NRTL and three-suffix Margules models, and also by ideal assumption. The best result was observed for the three-suffix Margules model, with a root mean square deviation (RMSD) equal to 0.26.

Graphical Abstract



Extended author information available on the last page of the article

Keywords Solid–liquid equilibrium · Phase diagrams · Fatty acids · Fatty alcohol compounds · Differential scanning calorimetry · Optical microscope

Abbreviations

ARD	Average relative deviation
DSC	Differential scanning calorimetry
NRTL	Non-random two-liquid model
RMSD	Root mean square deviation
SLE	Solid–liquid equilibrium
SSS	Tristearin
TAG	Triacylglycerols

Introduction

The worldwide production and consumption of oils and fats are growing over the years, and they are a source of energy and play an important role in human nutrition. Oils and fats are a multicomponent system composed of triacylglycerols (TAGs) and their minor constituents as free fatty acids and fatty alcohol compounds that can affect physical properties, such as texture, and polymorphic forms. (Wright and Marangoni 2005; Maximo et al. 2013; Matos et al. 2015).

TAGs are formed by a chemical bond of three fatty acids to a molecule of glycerol. The type and positioning of fatty acids within a TAG determines their melting behavior, which is especially significant to food industries, since it can affect texture and spreadability, for example (Wright and Marangoni 2005).

Tristearin, the TAG used in this study, is one of the major constituents of vegetable oils, readily available on high purity. Its crystalline behavior is well known for presenting three major crystalline forms: α -crystallite, which is the most prominent and kinetically stable, β - and β' -crystallite, which are thermodynamically stable (Da Silva et al. 2016). Besides, this TAG is used as hardstock to produce trans-free fat bases for shortenings and bakery margarines (Kellens et al. 1991; Oh et al. 2002; Matovic et al. 2005; Webster et al. 2018).

Fatty acids are carboxylic acids with an alkyl chain ranging from four to 36 carbons (C_4 – C_{36}), considered phase change materials due to their high-energy storage density (Wei et al. 2014; Zhao et al. 2014; Zhang et al. 2015). They can be used in food and cosmetic formulation and also to produce biodiesel and lubricants (Inoue et al. 2004a, b; Eckert et al. 2016). Fatty alcohol compounds are classified as long chain aliphatic alcohols, with six or more carbon atoms (Fisk et al. 2009). Concerning their use in industry, they are generally used to produce emulsifiers, emollients, and thickeners applied in food and cosmetic formulations (Johnson 1988; Kogan and Garti 2006; Perneti et al. 2007).

The use of fat compounds in different fields requires the understanding of their phase and mixture phase behavior, which is possible by the study of solid–liquid equilibrium (SLE). SLE can provide information regarding the interaction between different acyl chains, helping to determine the physical properties and the phase behavior of complex lipids and their mixtures (Inoue et al. 2004a, b; Dorighello Carareto et al. 2015). Thus, SLE allows the development and validation of models for better understanding the crystallization, fractionation, melting, and stabilization processes of fatty mixtures (Tadie et al. 2013; Matos et al. 2015).

SLE phase diagrams of fatty mixtures can be experimentally determined by several techniques, such as differential scanning calorimetry (DSC), X-ray, and optical microscopy. DSC determines the phase transition temperatures, which enables the determination of eutectic and monotectic points in phase diagram construction (Wesdorp 1990; Maximo et al. 2014a, b; Matos et al. 2016; Pelaquim et al. 2019). In addition, DSC is a fast, accurate, and reliable technique, requiring small amounts of sample.

This work came to complement previous published research that studied the SLE phase diagrams of TAGs + (fatty acids or fatty alcohol compounds) (Maximo et al. 2013; Matos et al. 2015, 2016; Pelaquim et al. 2019). Thus, the SLE behavior of six different binary mixtures measured by DSC technique are presented. Some thermal transitions were evaluated with the aid of an optical microscope linked to a temperature controller. The components chosen were: tristearin (1) as TAG and capric acid (2), lauric acid (3), myristic acid (4), 1-decanol (5), 1-dodecanol (6), and 1-tetradecanol (7). The parameters of three-suffix Margules and NRTL models were adjusted to the experimental data to describe the *liquidus lines* of the studied systems.

Experimental methods

Materials

High pure components (Table 1) were used to prepare the binary mixtures without further purification. The DSC calibration was carried out considering onset temperatures, using a heating rate of 1 K min^{-1} and the following standards: indium (≥ 0.990 molar fraction, CAS number 7440-74-6) from TA Instruments; naphthalene (≥ 0.990 molar fraction, CAS number 91-20-3) from Fluka Analytical (Germany); and cyclohexane (≥ 0.990 molar fraction, CAS number 110-82-7) from Sigma-Aldrich (USA).

Table 1 Sources and purities of the compounds used in this study

Chemical Name	CAS number	Mass fraction purity ^a	Source
Tristearin	555–43-1	> 0.990	Sigma-Aldrich (USA)
Capric acid	334–48-5	> 0.990	Sigma-Aldrich (USA)
Lauric acid	143–07-7	> 0.990	Sigma-Aldrich (USA)
Myristic acid	544–63-8	> 0.990	Sigma-Aldrich (USA)
1-decanol	112–30-1	> 0.990	Sigma-Aldrich (USA)
1-dodecanol	112–53-8	> 0.990	Sigma-Aldrich (USA)
1-tetradecanol	112–72-1	> 0.990	Sigma-Aldrich (USA)

^aAs indicated by the supplier

Apparatus and procedure

Binary mixture preparation

Binary mixtures were prepared by weighting known quantities of each compound using an analytical scale with a precision of $\pm 2 \times 10^{-4}$ (Shimadzu AU220, Japan), totalizing 0.50 g of each mixture, to obtain the entire range of the phase diagram composition in increments of 0.1 or 0.2 tristearin molar fractions. A Thermoprep equipment (Metrohm, Herisau), the oven used for Karl Fischer titration, was used to melt the samples, and ensure their complete homogenization under a nitrogen atmosphere. After melting, the samples were cooled down to room temperature and kept under refrigeration until their use in the DSC equipment. The uncertainty obtained due to error propagation from the weighted masses was estimated as not higher than 6×10^{-4} (in molar fraction).

Differential scanning calorimetry (DSC)

SLE experimental data (melting temperatures and enthalpies of fusion) of the binary mixtures were determined on a Differential Scanning Calorimetry equipment (MDSC 2920, TA Instruments, New Castle) equipped with a refrigerated cooling system operated in a temperature range from 248 to 360 K; high-purity nitrogen was used as purge gas at 50 mL/min. The melting temperature and heat flow were previously calibrated with the primary calibration standards: indium (certificated by TA Instruments), naphthalene (Fluka Analytical, Germany), and cyclohexane (Sigma Aldrich, USA), with purity greater than 0.99 mass fraction, at a heating rate of 1 K min^{-1} for at least three times with each calibration. The standard deviations of the measurements ranged from 0.07 to 0.1 K.

Each sample mixture was weighed (4–7 mg) using a microanalytical scale with 2×10^{-6} accuracy (AD6, PerkinElmer, Waltham) and sealed in aluminum pans. The samples were submitted to a thermal treatment according

to Costa et al. (2007) to erase previous thermal histories because of the fatty compound polymorphism effects. The thermal treatment consisted of a heating step at 5 K min^{-1} from room temperature until 15 K above the melting point of the fat compound with the highest melting point of the mixture, followed by an isothermal time of 20 min; a cooling run at 1 K min^{-1} up to 25 K below the smaller melting point of the fat compound with the lower melting point of the mixture and another isothermal step of 30 min. After this thermal treatment, the run for data acquisition was done at a heating rate of 1 K min^{-1} .

Thermal event temperatures were analyzed using the TA Universal Analysis software. The transitions, eutectic, and melting temperatures was calculated through the peak temperature and the enthalpy was calculated from the area of the corresponding peak (Costa et al. 2007). Onset temperature is more recommended to find the melting temperature due to its low dependence on heating rate and sample parameters. However, the use of onset temperature to determine the melting peak may be inaccurate due to the influence of other peaks and overlapped peaks in the differential thermal curve that are generally observed in fatty compounds added to low values of heat transfer coefficient especially observed in mixtures of organic compounds (Höhne et al. 2003; Costa et al. 2007). Therefore, in this work we used peak temperature because of better repeatability and ease determination.

Triplicate runs were done for some selected compositions to verify the repeatability of the temperatures attributed to each thermal event and the reliability of the methodology and equipment. It was observed that all the uncertainties of fusion temperature for pure components and binary mixtures were below 0.30 K, indicating that the DSC equipment presents a good reproducibility. For a better visualization, the triplicate of SSS + C14OH at $x_1 = 0.40$ are presented in the Supplementary Information, as well as the comparison between the peak temperature of each event (Figure S7 and Table S1). One can observe that the results of the temperatures determined for the endothermic and exothermic peaks remain very close.

Optical microscopy

An optical microscope (Leica DM 2700 M, China) with a temperature controller (Linkam LTS 420, United Kingdom) was used to evaluate the solid–liquid transitions of some selected binary mixtures. The sample amount used for this experiment was approximately 50 mg. A heating rate of 0.1 K min^{-1} was employed from 10 degrees under the eutectic temperature until reaching the sample melting temperature. Images were captured every 60 s with a magnification of 10 or 20 times.

SLE thermodynamic modelling

To describe the *liquidus* lines of the binary mixture, the activity coefficient was calculated by three-suffix Margules and NRTL models, considering the ideal behavior of the liquid phase. The models were used in Eq. 1 as discussed by Prausnitz et al. (1999), where the solid–solid transitions and molar heat capacity of pure components were not considered. Moreover, the activity coefficient of component i in the solid phase at equilibrium was replaced by the activity coefficient of the pure component ($x_i^s \gamma_i^s = 1$), representing the immiscibility of both components in that phase.

$$\ln \frac{1}{x_i^L \gamma_i^L} = \frac{\Delta_{fus,i} H}{RT_{m,i}} \left(\frac{T_{m,i}}{T} - 1 \right), \quad (1)$$

where x_i^L is the molar fraction of component i in the liquid (L) phase; γ_i^L is the activity coefficient of component i also in the liquid phase; $\Delta_{fus,i} H$ is the fusion enthalpy at the melting temperature of component i ; $T_{m,i}$ is the melting temperature of component i ; T is the calculated temperature; and R is the universal gas constant.

The parameters of three-suffix Margules and NRTL models were adjusted to find the activity coefficients of the liquid phase (Prausnitz et al. 1999). Downhill simplex optimization method (Vetterling et al. 1992) was used to determine the models' parameters with the objective function (S) given in Eq. 2, where (N) is the number of experimental measurements and (σ_n) is the temperature uncertainty, as proposed by Costa et al. 2007. The root mean square deviation (RMSD) was used to evaluate the deviation between the calculated temperature and the experimental ones.

$$S = \frac{1}{2} \sum_{i=1}^N \left(\frac{T_i^{\text{exp}} - T_i^{\text{cal}}}{\sigma_n} \right)^2 \quad (2)$$

Results and discussion

Pure tristearin thermal properties

The thermal properties of fatty acids and fatty alcohol compounds were previously presented (Pelaquim et al. 2019). Thus, Table 2 shows the transition temperatures of tristearin, which are represented by exothermic peaks or endothermic peaks, due to events such as residual melting temperature or polymorphs transformation; the melting temperature, which is the endothermic peak that occurs at higher temperature; the molar enthalpy of fusion; and the experimental standard deviations presented in parentheses, as well as the literature data of tristearin. These data were done in triplicate and standard deviation was calculated according to Eq. 3.

$$s_x = \sqrt{\frac{\sum_{i=1}^n (x_i - x')^2}{n - 1}}, \quad (3)$$

where s_x is the standard deviation, n is the number of data points, x_i is each of the values of the data, and x' is the mean value of x_i .

Equation 4 was used to calculate the average relative deviation (ARD), which consists of the deviation between the melting temperature and molar enthalpies determined in this study ($\Gamma_{\text{This study}}$) and in the literature ($\Gamma_{\text{Literature}}$).

Table 2 Thermal properties of tristearin: transition temperatures (T_{trans}); melting temperatures (T_{m}); molar enthalpy of fusion (ΔH_{fus}); and literature data, $p = 94.6$ kPa

Component	T_{trans}/K		T_{m}/K		$\Delta H_{\text{fus}}/(\text{kJ mol}^{-1})$	
	This study	Literature	This study	Literature	This study	Literature
Tristearin	328.72 (± 0.08)	328.27 (Costa et al. 2010)	345.86 (± 0.11)	345.76 (Costa et al. 2011)	198.56 (± 3.36)	–
	330.87 ^a (± 0.41)	329.51 (Costa et al. 2010)		345.27 (Costa et al. 2010)		–
	331.68 (± 0.46)	332.33 (Costa et al. 2010)		346.60 (Yui et al. 2017)		195.30 (Yui et al. 2017)
				345.90 (Matovic et al. 2005)		197.55 (Matovic et al. 2005)
				344.35 (Kellens and Reynaers 1992)		190.00 (Kellens and Reynaers 1992)

Uncertainties Type A

^aTemperature of exothermic transition peak

$$\text{ARD} = \left(\frac{1}{N} \sum_{i=1}^n \frac{|\Gamma_{\text{This study}} - \Gamma_{\text{Literature}}|}{\Gamma_{\text{This study}}} \right) \times 100. \quad (4)$$

The ARD of melting temperature and the ARD of molar enthalpy were 0.17% and 2.15%, respectively. Both results show a good agreement between our experimental data and literature data.

TAGs are well known by their ability to crystallize under different crystal forms (Garti and Sato 1988). The most common ones are α , β' , and β forms, in which α is the less stable and β is the most stable form (Timms 1984; Persson 2008). The generation of tristearin β' -form is possible only under a special thermal conditioning treatment because of the speediness of the α to β -form transformation (Singh et al. 1999).

Figure 1 compares the DSC curve of tristearin determined in this study and that the one determined by Singh et al. 1999 using a heating rate equal to 2.5 K min^{-1} . One can observe that the curve determined in this study is similar to the tristearin curve from the literature, showing four well-defined peaks (Timms 1984; Singh et al. 1999; Persson 2008) despite the different heating rate and thermal treatment used by the authors. According to the literature (Singh et al. 1999), the first peak observed in Fig. 1 is an endothermic peak that indicates a residual α -form melting at 328.61 K (peak number 1 indicated by the black arrow). This endothermic peak is followed by an exothermic one observed at 330.42 K, which is attributed to the transformation from α -form to β -form (peak number 2). Peak number 2 is overlapped by peak number 3, which is a residual β -form crystallization at 332.84 K; and peak

number 4 is related to tristearin β -form melting temperature, at 345.73 K.

Experimental SLE data

Six SLE phase diagrams were constructed in this study, formed by tristearin + fatty acids (capric acid, lauric acid, and myristic acid) and tristearin + fatty alcohol compounds (1-decanol, 2-dodecanol, and 1-tetradecanol). The experimental data are shown in Tables 3, 4, 5, 6, 7 and 8, where x_1 corresponds to tristearin molar fraction. The thermal curves are presented in the Supplementary Information (Figs. S1 to S6).

Phase diagrams and microscopy analysis of tristearin + fatty acids

Figure 2 presents the phase diagram of tristearin + fatty acids. All of these systems present a monotectic behavior that was also observed in the literature for tristearin + rice bran oil system (Humphrey and Narine 2005; Costa et al. 2010). All the phase diagrams presented in Fig. 2 present a monotectic behavior; however, the exact composition of such point is not known due to its proximity to the pure fatty acid (Inoue et al. 2004a, b). Nevertheless, the *liquidus line* calculated using the ideal approach, three-suffix Margules, and NRTL models for the tristearin (1) + myristic acid (4) system indicated the presence of a eutectic point at 0.02 tristearin molar fraction. The model results suggest the occurrence of a eutectic reaction (Fig. 2C) and once more the proximity of pure myristic acid makes its composition determination by DSC a hard task.

Fig. 1 Tristearin differential thermal curves

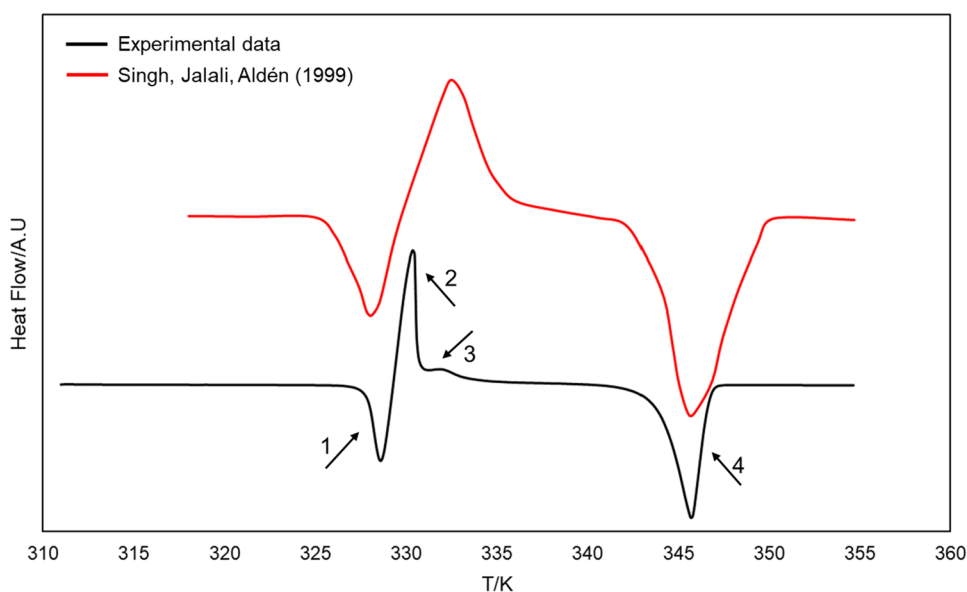


Table 3 Experimental solid–liquid equilibrium data of the tristearin (1) + capric acid (2) system at $p = 94.6$ kPa

x_1	$T_{\text{trans}}/\text{K}$	T_{eut}/K	T_{m}/K	$T_{\text{trans,pure1}}/\text{K}$	$T_{\text{trans,pure2}}/\text{K}$	$T_{\text{trans,pure3}}/\text{K}$	Solid Phase
0.0000			305.22 (Pelaquim et al. 2019)				Capric acid
0.1997		304.86	339.62				Tristearin
0.4002		304.63	342.35				Tristearin
0.5998	301.14	303.75	343.93				Tristearin
0.8010		303.53	345.20				Tristearin
1.0000			345.86	328.72	330.87 ^a	331.68 ^a	Tristearin

Solid–solid transitions (T_{trans}), eutectic temperature (T_{eut}), melting temperature (T_{m}), pure component transition temperatures ($T_{\text{trans,pure}}$)

Uncertainties Type A are $u(x) = 0.0006$, $u(T) = 0.3$ K, and $u(p) = 0.3$ kPa

^aTemperature of exothermic peak transition

Table 4 Experimental solid–liquid equilibrium data of the tristearin (1) + lauric acid (3) system at $p = 94.6$ kPa

x_1	$T_{\text{trans}}/\text{K}$	T_{eut}/K	T_{m}/K	$T_{\text{trans,pure1}}/\text{K}$	$T_{\text{trans,pure2}}/\text{K}$	$T_{\text{trans,pure3}}/\text{K}$	Solid Phase
0.0000			318.50 (Pelaquim et al. 2019)				Lauric acid
0.1000		317.13	335.85				Tristearin
0.2000		317.58	339.29				Tristearin
0.4002	344.71	317.06	342.07				Tristearin
0.6001		314.84	345.16				Tristearin
0.7994	331.45 ^b	316.57	344.23				Tristearin
1.0000			345.86	328.72	330.87 ^a	331.68 ^a	Tristearin

Solid–solid transitions (T_{trans}), eutectic temperature (T_{eut}), melting temperature (T_{m}), pure component transition temperatures ($T_{\text{trans,pure}}$)

Uncertainties Type A are $u(x) = 0.0006$, $u(T) = 0.3$ K, and $u(p) = 0.3$ kPa

^aTemperature of exothermic peak transition

Table 5 Experimental solid–liquid equilibrium data of the tristearin (1) + myristic acid (4) system at $p = 94.6$ kPa

x_1	$T_{\text{trans}}/\text{K}$	T_{eut}/K	T_{m}/K	$T_{\text{trans,pure1}}/\text{K}$	$T_{\text{trans,pure2}}/\text{K}$	$T_{\text{trans,pure3}}/\text{K}$	Solid Phase
0.0000			329.05 (Pelaquim et al. 2019)				Myristic acid
0.1001		326.90	335.43				Tristearin
0.1999		327.11	338.86				Tristearin
0.4001	319.10 ^b	326.53	342.16				Tristearin
0.6001	321.22 ^b	325.80	343.82				Tristearin
0.7999	321.05 ^b	324.08	344.71				Tristearin
1.0000			345.86	328.72	330.87 ^a	331.68 ^a	Tristearin

Solid–solid transitions (T_{trans}), eutectic temperature (T_{eut}), melting temperature (T_{m}), pure component transition temperatures ($T_{\text{trans,pure}}$)

Uncertainties Type A are $u(x) = 0.0006$, $u(T) = 0.3$ K, and $u(p) = 0.3$ kPa

^aTemperature of exothermic peak transition

The ideal model underestimated the *liquidus line* for all three phase diagrams but follow the same trend of the experimental data. Three-suffix Margules, and NRTL models presented a much better match with the *liquidus line*, in which the lines almost overlapped the experimental dots.

The phase diagrams also show that the solid–liquid region decreases with the fatty acids chain length increase. Thus, tristearin (1) + capric acid (2) system presented the bigger solid–liquid region and tristearin (1) + myristic acid (4) system the smaller region. Concerning the phase diagrams

Table 6 Experimental solid–liquid equilibrium data of the tristearin (1) + 1-decanol (5) system at $p=94.6$ kPa

x_1	$T_{\text{trans}}/\text{K}$	T_{eut}/K	T_m/K	$T_{\text{trans,pure}}/\text{K}$	$T_{\text{trans,pure}2}/\text{K}$	$T_{\text{trans,pure}3}/\text{K}$	Solid Phase
0.0000			279.84 (Pelaquim et al. 2019)				1-decanol
0.1001		279.76	338.20				Tristearin
0.2001		278.62	339.17				Tristearin
0.3996	322.82 ^b	276.52	342.06				Tristearin
0.6010		274.62	344.31				Tristearin
0.7989	328.28		345.55				Tristearin
1.0000			345.86	328.72	330.87 ^a	331.68 ^a	Tristearin

Solid–solid transitions (T_{trans}), eutectic temperature (T_{eut}), melting temperature (T_m), pure component transition temperatures ($T_{\text{trans,pure}}$)

Uncertainties Type A are $u(x)=0.0006$, $u(T)=0.3$ K, and $u(p)=0.3$ kPa

^aTemperature of exothermic peak transition

Table 7 Experimental solid–liquid equilibrium data of the tristearin (1) + 1-dodecanol (6) system at $p=94.6$ kPa

x_1	T_{eut}/K	T_m/K	$T_{\text{trans,pure}}/\text{K}$	$T_{\text{trans,pure}2}/\text{K}$	$T_{\text{trans,pure}3}/\text{K}$	Solid Phase
0.0000		297.78 (Pelaquim et al. 2019)				1-dodecanol
0.1000	296.50	337.38				Tristearin
0.1998	296.45	339.57				Tristearin
0.4002	295.16	341.19				Tristearin
0.5995	295.49	343.17				Tristearin
0.8001	296.39	344.56				Tristearin
1.0000		345.86	328.72	330.87 ^a	331.68 ^a	Tristearin

Solid–solid transitions (T_{trans}), eutectic temperature (T_{eut}), melting temperature (T_m), pure component transition temperatures ($T_{\text{trans,pure}}$)

Uncertainties Type A are $u(x)=0.0006$, $u(T)=0.3$ K, and $u(p)=0.3$ kPa

^aTemperature of exothermic peak transition

Table 8 Experimental solid–liquid equilibrium data of the tristearin (1) + 1-tetradecanol (7) system at $p=94.6$ kPa

x_1	$T_{\text{trans}}/\text{K}$	$T_{\text{trans}2}/\text{K}$	T_{eut}/K	T_m/K	$T_{\text{trans,pure}}/\text{K}$	$T_{\text{trans,pure}2}/\text{K}$	$T_{\text{trans,pure}3}/\text{K}$	Solid Phase
0.0000				310.71 (Pelaquim et al. 2019)				1-tetradecanol
0.1000			311.03	337.48				Tristearin
0.1999	309.60	312.70	310.88	339.21				Tristearin
0.4004	308.84	312.52	310.51	341.87				Tristearin
0.5999	309.73		311.66	343.41				Tristearin
0.7997		321.06 ^b		344.86				Tristearin
1.0000				345.86	328.72	330.87 ^a	331.68 ^a	Tristearin

Solid–solid transitions (T_{trans}), eutectic temperature (T_{eut}), melting temperature (T_m), pure component transition temperatures ($T_{\text{trans,pure}}$)

Uncertainties Type A are $u(x)=0.0006$, $u(T)=0.3$ K, and $u(p)=0.3$ kPa

^aTemperature of exothermic peak transition

regions, in Fig. 2C is possible to identify the region 1 above of *liquidus line* composed by a liquid phase, region 2 that is a solid–liquid equilibrium domain composed by solid tristearin with a liquid phase, region 3 below of the *solidus line* formed by a solid mixture of both components

and region 4 formed by a solid solution of the mixture components.

To better understand and evaluate this behavior and the transitions, optical microscope images were captured at 0.2000 and 0.9000 tristearin molar fractions of tristearin

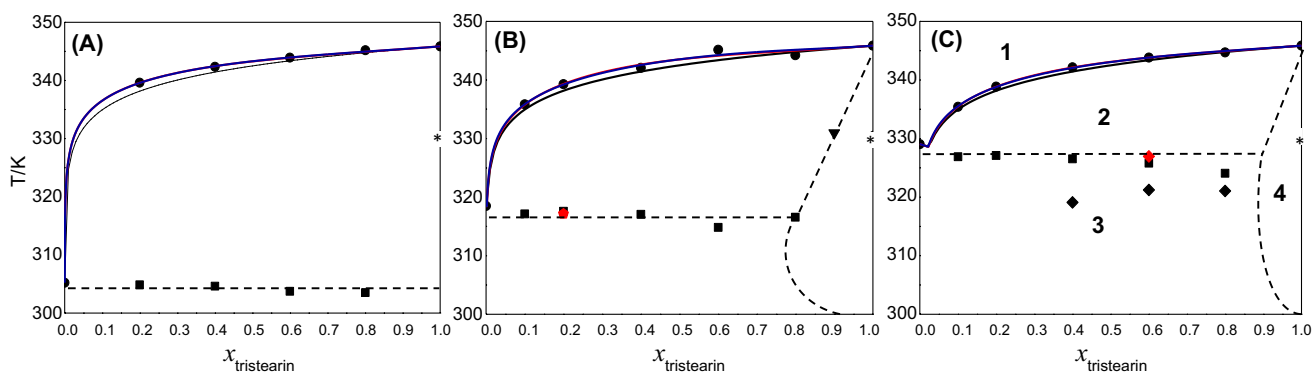


Fig. 2 SLE phase diagram of the **A** tristearin (1)+capric acid (2) system; **B** tristearin (1)+lauric acid (3) system; **C** tristearin (1)+myristic acid (4) system: (filled circle) melting temperature; (filled square) eutectic reaction temperature; (filled diamond) exothermic transition

temperature; (filled diamond) melting process from optical microscopy; (*) pure component transition temperature; (grey line) ideal model; (red line) three-suffix Margules; (blue line) NRTL; (dashed line) guide to the eyes

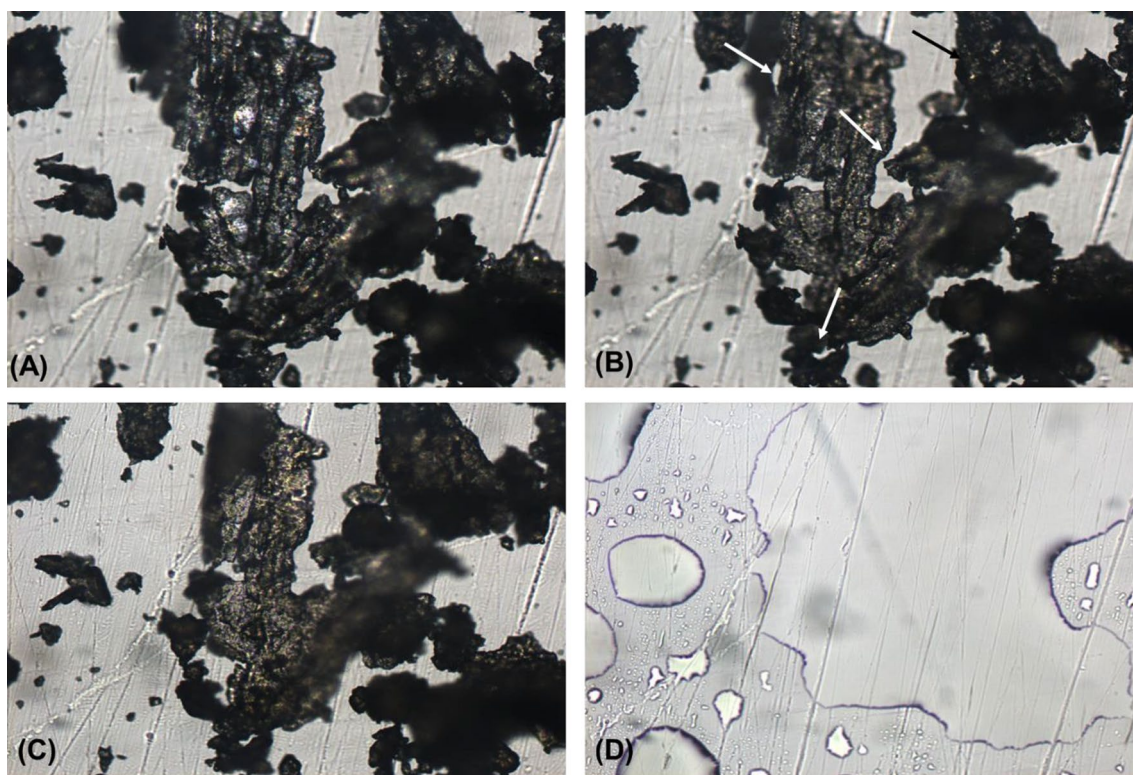


Fig. 3 Optical micrographs of the tristearin (1)+lauric acid (3) system at $x_l=0.2000$ with **A** 315.15 K; **B** 317.15 K; **C** 320.45 K; **D** 345.65 K. Magnification of 20 \times

(1)+lauric acid (3) system, presented in Figs. 3 and 4, and at 0.6000 and 0.7999 tristearin molar fractions of tristearin (1)+myristic acid (4) system, presented in Figs. 5 and 6.

Figure 2C, tristearin (1)+myristic acid (4) system, also shows exothermic events observed in DSC curves at tristearin molar fractions of 0.4001, 0.6001, and 0.7999, approximately. The exothermic peaks around 320 K probably indicate the α -form crystallization of tristearin (Kellens,

Reynaers 1992). Besides, tristearin (1)+myristic acid (4) and tristearin (1)+lauric acid (3) systems present a solid solution starting at about 0.7999 molar fraction. Optical microscope images were captured to better explain this behavior (Figs. 5 and 6).

In Fig. 3A, the mixture of tristearin (1)+lauric acid (3) is in a solid phase at 315.15 K. With the increase of temperature, the mixture starts to melt at 317.15 K, as shown

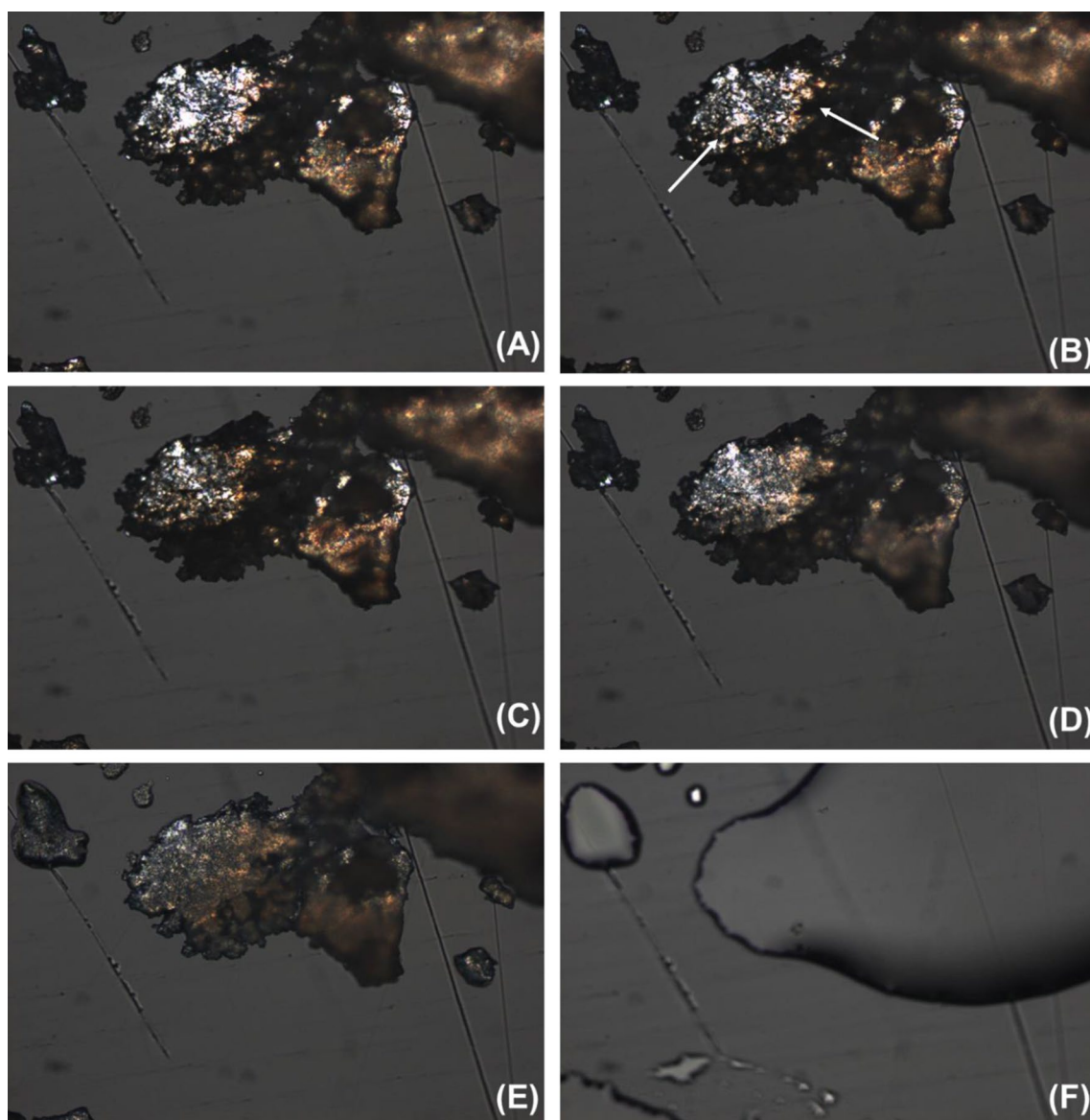


Fig. 4 Optical micrographs of the tristearin (1)+lauric acid (3) system at $x_1=0.9000$ with **A** 313.35 K; **B** 314.05 K; **C** 317.35 K; **D** 330.95 K; **E** 346.65 K; **F** 347.45 K. Magnification of 20 \times

by the white arrows (Fig. 3B), indicating that solid lauric acid coexists with the liquid mixture. The mixture remains in both solid and liquid phases, almost without change until 320.45 K, where the melting process became noticeable again (Fig. 3C). This behavior indicates the occurrence of a monotectic behavior. After that, the temperature increase promotes the complete melting of the mixture at 345.65 K (Fig. 3D).

Initially, the tristearin (1) + lauric acid (3) system at 0.9000 tristearin molar fraction was in solid phase at 313.35 K, as indicated by Fig. 4A. Increasing the temperature up to 314.05 K, it is easy to note the brightness loss of the sample, as indicated by the white arrows in Fig. 4B.

This phenomenon can be explained by a recrystallization probably due to a change in the crystal form of the mixture. This process continues until 317.35 K. The mixture remains in a solid phase (Fig. 4C) up to almost 330.95 K. This behavior can be related to tristearin polymorphism. When the temperature reaches 330.95 K, the mixture starts the melting process, which is perceptible by the increase in sample brightness in Fig. 4D, and the melting process only stops with the complete sample melting at 347.45 K. The fact that a liquid and a solid phase coexistence was not seen from 317 K in this mixture indicates the presence of a solid solution in the tristearin-rich region of the phase diagram, as shown in Fig. 2 (B) by the dotted lines (guide to the eyes).

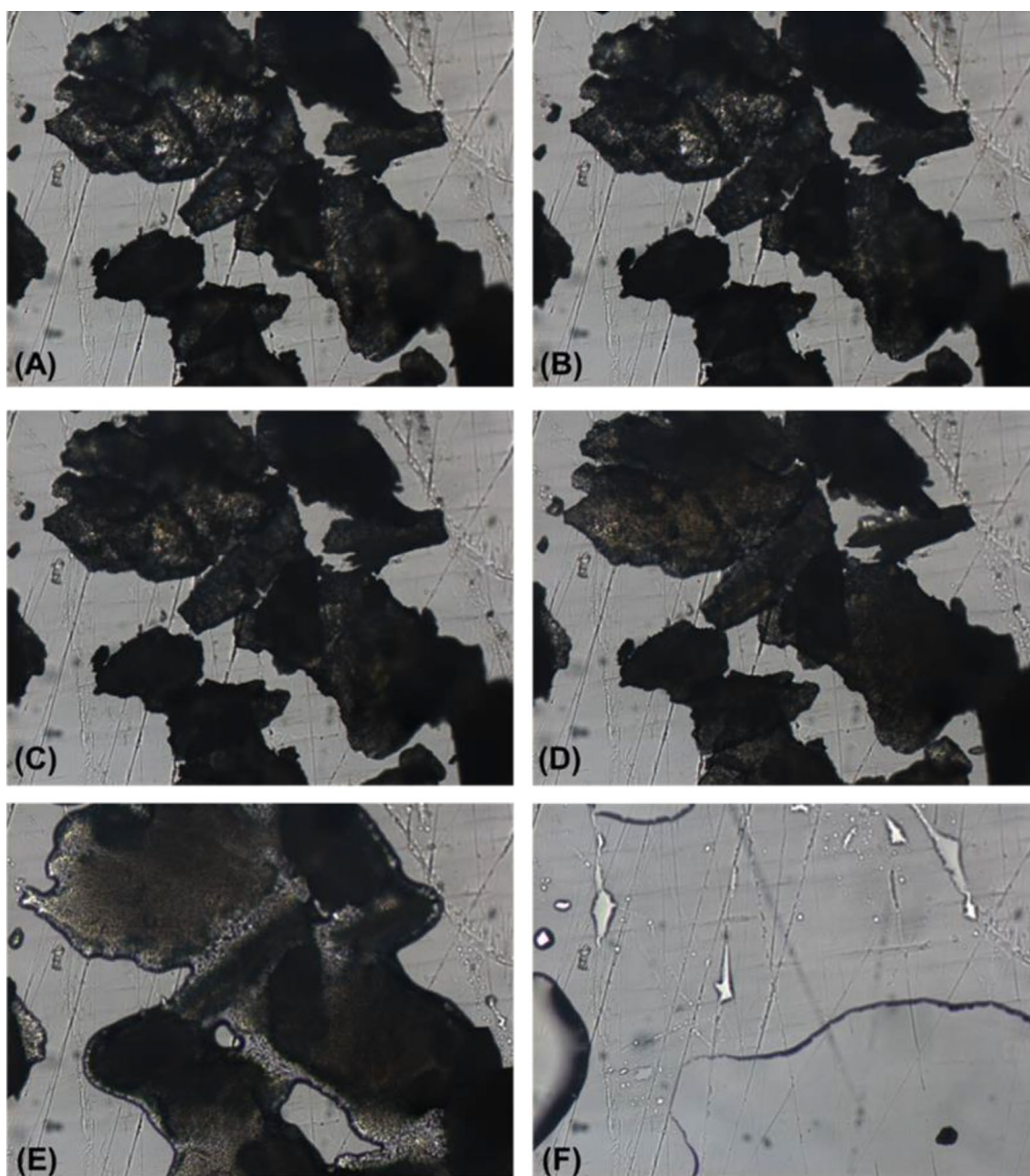


Fig. 5 Optical micrographs of the tristearin (1) + myristic acid (4) system at $x_1=0.6000$ with **A** 318.15 K; **B** 318.45 K; **C** 326.95 K; **D** 344.45 K; **E** 345.65 K; **F** 346.35 K. Magnification of 20 \times

Some images were also captured for tristearin (1) + myristic acid system and are presented in Fig. 5. The image taken at 318.15 K shows the sample in a solid state (Fig. 5A); the temperature increase at 318.45 K makes it possible to note that the crystals became darker, indicating a recrystallization process into a new solid phase through which it is more difficult to pass light (Fig. 5B). This transition was also observed in the differential thermal curves at 321.22 K (Fig. S3 in the Supplementary Information), and it was plotted in the phase diagram (Fig. 2C), represented by the dark diamond

symbol. The melting process begins at 326.95 K, as shown in Fig. 5C, and, at this composition and temperature, liquid myristic acid coexists with a solid phase mixture. The melting process continues with the temperature increase until total sample melting at 346.35 K (Fig. 5D–F).

In Fig. 6B, one can observe the recrystallization discussed before. The temperature increase made the sample become darker, which is very clear in Fig. 6A–C, from 318.15 up to 344.45 K. However, at this sample composition, the melting process does not start at about 327 K, but only

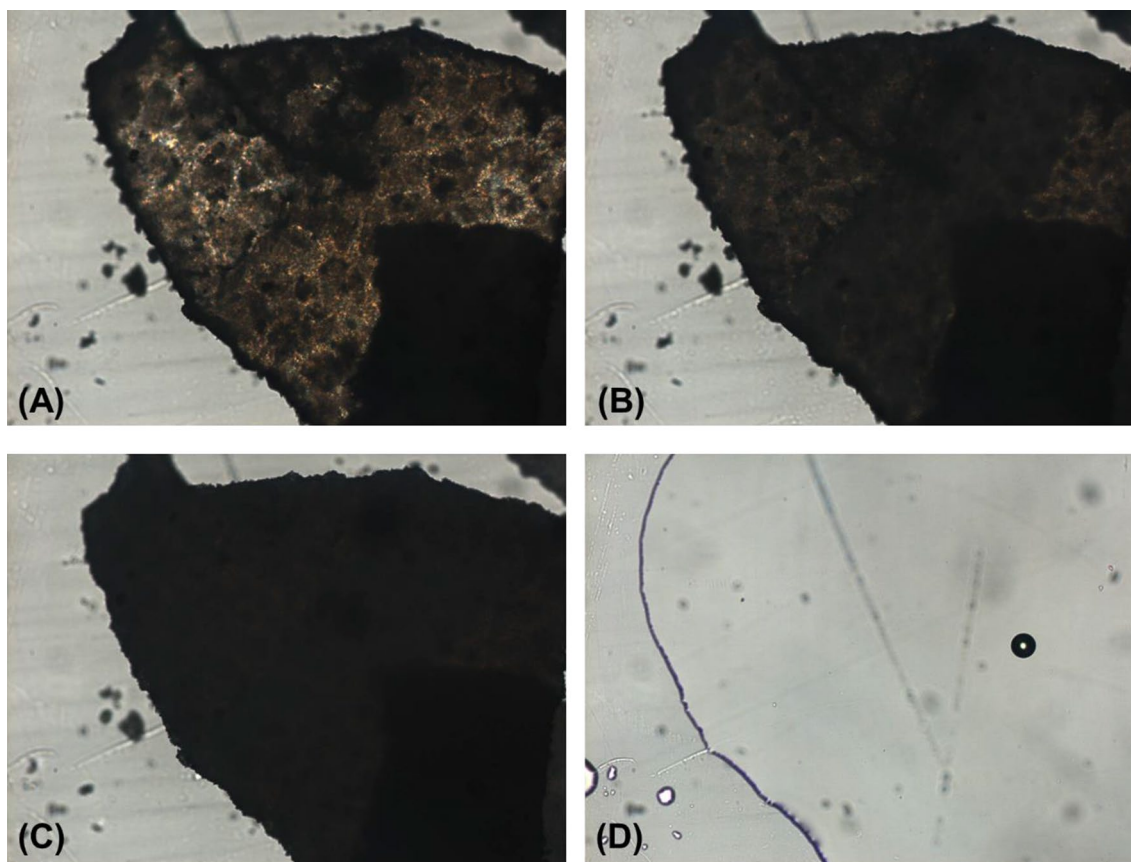


Fig. 6 Optical micrographs of the tristearin (1) + myristic acid (4) system at $x_1 = 0.7999$ with **A** 318.15 K; **B** 326.15 K; **C** 344.45 K; **D** 346.35 K. Magnification of 20 \times

at 344.45 K, approximately 18 degrees above the thermal events observed by DSC, and the sample is totally melted at 346.35 K (Fig. 6D). Thus, the images confirm the formation of a solid solution in the extreme of the phase diagram that is rich in tristearin, since it was not observed a coexistence of a liquid + solid phase from 327 K, approximately, which is the assumed eutectic reaction temperature.

To understand the behavior of different TAGs on SLE phase diagram with fatty acids, the *liquidus* line determined in this study containing tristearin (1) + myristic acid (4) was plotted with three *liquidus* lines previously determined, containing tripalmitin + myristic acid (Pelaquim et al. 2019), trilaurin + myristic acid (Matos et al. 2016), and triolein + myristic acid (Matos et al. 2015), as shown in Fig. 7.

Considering the melting point of myristic acid, one can observe two different behaviors of the *liquidus* line. The first one is observed for tristearin or tripalmitin + myristic acid systems (Fig. 7A), in which the eutectic point moves from $x_{\text{myristic acid}} \cong 0.90$ to $x_{\text{myristic acid}} \cong 1.00$, a monotectic point. The second one is observed for trilaurin or triolein + myristic acid systems (Fig. 7B); in this case, the eutectic point moves from $x_{\text{myristic acid}} \cong 0.50$ to $x_{\text{myristic acid}} \cong 0.00$, a monotectic point. The eutectic point moves in the direction of the pure

compound with the smaller melting temperature, in the case of saturated TAGs in the direction of the smaller carbon chain length TAG, as previously reported for systems formed by triolein and trilaurin + fatty alcohol compounds or fatty acids (Maximo et al. 2019).

Phase diagrams and microscopy analysis of tristearin + fatty alcohol compounds

DSC curves and phase diagram of tristearin (1) + 1-tetradecanol (7) system are presented in Figs. 8 and 9, respectively. Figure 8 shows that the DSC curves for the mixtures present at least two thermal events. The first thermal event, around 310 K, is attributed to the start of the phase change process, and the second, at highest temperature, represents the full sample melting. The TAG composition increase promotes a severe increase in the second endothermic peak and a significantly decrease in the first endothermic peak. As generally observed for fat systems (Carareto et al. 2014; Matos et al. 2015), here it is also note the occurrence of overlapped peaks at 0.1999, 0.4004, 0.5999, and 0.7997 tristearin molar fractions, at lower temperature (first peak), as indicated by the black arrows in Fig. 8. The overlapped peaks can be

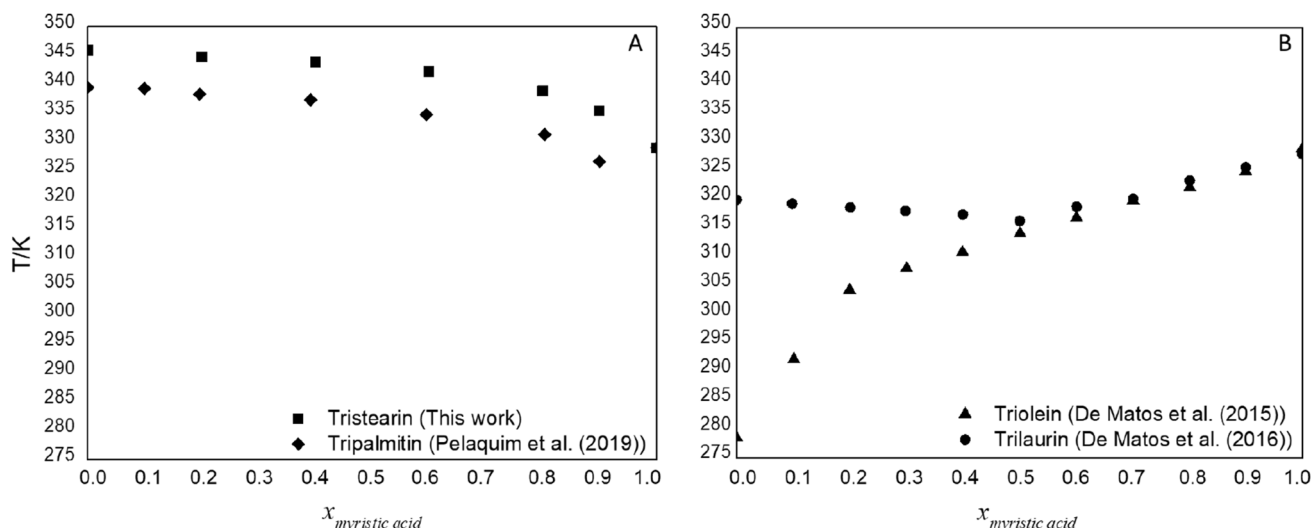


Fig. 7 Liquidus line of **A** tripalmitin + myristic acid, and tristearin + myristic acid; **B** trilaurin + myristic acid and triolein + myristic acid

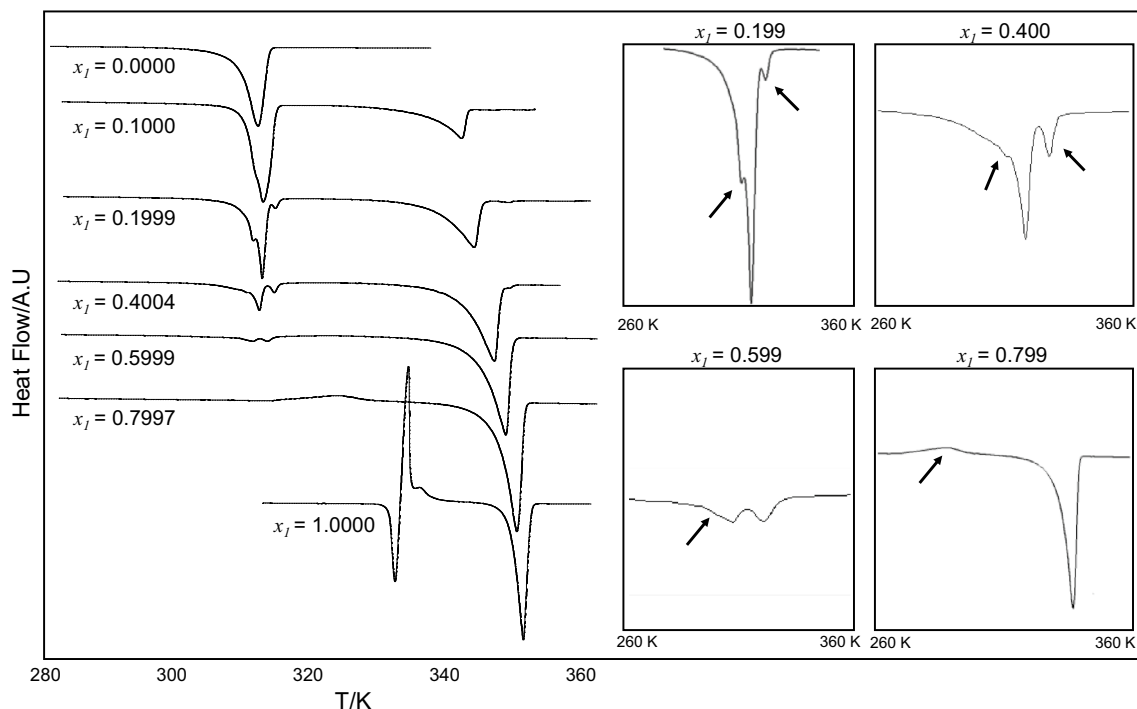


Fig. 8 Tristearin (1) + 1-tetradecanol (7) system DSC curves

related to the melting of tristearin polymorphs, and the small spread exothermic peak at the 0.7997 tristearin molar fraction is probably due to tristearin α -form crystallization (Kellens and Reynaers 1992). Even though the peaks are overlapped, the most pronounced peak observed at 311 K has its intensity increased with the rise in tristearin molar fraction, as it happens for eutectic systems (Inoue et al. 2004a, b).

According to the literature (Craven and Lencki 2011), in this case the phase diagram is apparently considered to present a monotectic behavior (Fig. 9). Thus, to better understand and evaluate this behavior, microscope optical images were taken at 0.1999 and 0.7997 tristearin molar fractions.

Initially, the binary mixture of tristearin (1) + 1-tetradecanol (7) at 0.1999 tristearin molar fraction is solid at

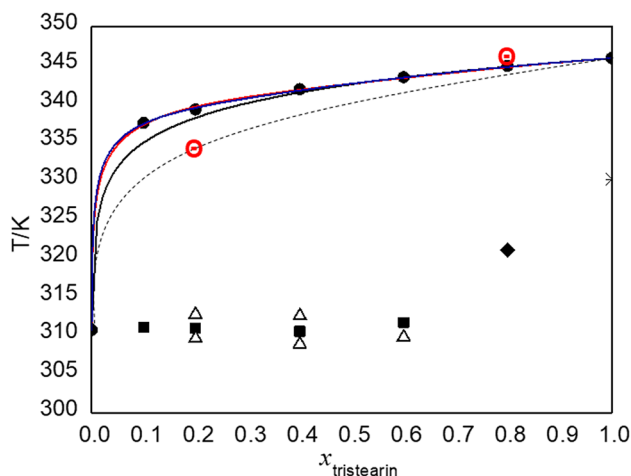


Fig. 9 SLE phase diagram of the tristearin (1)+1-tetradecanol (7) system: (filled circle) melting temperature; (filled square) solid transition temperature; (filled diamond) exothermic transition temperature; (triangle) solid transition temperature; (*) pure component transition temperature; (⊖) solid–liquid transition temperature determined by optical microscope (black line) ideal model; (red line) three-suffix Margules; (blue line) NRTL; (dashed line) guide to the eyes of solid solution formation according to microscope results

305.25 K (Fig. 10A). With the temperature increase, we can note the progress of the crystallization process at 310.55 K (Fig. 10B), as observed for the previous systems. The crystallization process continues until 312.65 K and is perceptible due to brightness loss of the images from Fig. 10A to C. This process is confirmed by DSC curves in the region with the overlapped peaks around 311 K (Fig. 8). The peak temperatures of each overlapped peak were also plotted in the phase diagram using the Δ symbol (Fig. 9). Contrary to expectations, the solid phase remained up to 332.65 K (Fig. 10D), 30 degrees above the supposed solid–liquid transition temperature, as can be seen in the phase diagram presented in Fig. 9. A liquid phase in equilibrium with a solid phase can be clearly observed only at 332.65 K in Fig. 9E, represented by the \ominus symbol in the phase diagram (Fig. 9). Finally, at 344.05 K, the mixture is completely melted (Fig. 10F). This behavior agrees with the peak obtained by the DSC experiments, the peak observed at higher temperature. Thus, these images indicate that the tristearin (1) + 1-tetradecanol (7) system does not obey the description of a simple eutectic system. The images confirm the formation of a solid solution in all composition range, and as was observed, this solid solution goes through some changes in its solid phase due to a crystal restructuring (polymorphic change), clearly perceptible because of the crystal darkness with the temperature increase, as can be better seen in the gif 1 at the Supplementary Information. A better understanding of such behavior requires the use of other analysis techniques, such as x-ray diffraction, and it is not the main goal of this study.

The same behavior observed for the 0.1999 tristearin molar fraction was observed for the 0.7997 tristearin molar fraction of the same system (Fig. 11), i.e., a recrystallization process takes place at 316.35 K (Fig. 11B) and the melting process started at 345.85 K (Fig. 11C), very close to the *liquidus* line temperature. This result corroborates the previously discussed behavior and can be better seen in the gif 2 at the Supplementary Information.

Figure 12 shows the phase diagrams of tristearin (1) + 1-decanol (5) and tristearin (1) + 1-dodecanol (6) systems. One can observe that both systems present, according to the experimental data and microscopy analysis, the same characteristics of the previously discussed system. Therefore, these systems might also present a solid solution region in all molar fraction composition range.

In general, solid solution phase may occur in binary solid mixtures, when the two components are miscible in all proportions in a liquid state. The solid solution changes the behavior of the melting profile of the systems, especially the beginning of the melting temperature which difficult its identification by using DSC data (Maximo et al. 2019). In addition, the increase of the triacylglycerol carbon chain and the increase of the difference between the melting temperatures of the pure components leads to a larger solid solution region (Maximo et al. 2014a, b).

As for the systems with fatty acids, the ideal behavior underestimates the *liquidus* line of mixtures composed by tristearin + fatty alcohol compounds and three-suffix Margules and NRTL presented a good match. In Fig. 12A it is possible to observe the 3 regions composed by this kind of phase diagram: region 1 is formed by a liquid phase, region 2 is a solid–liquid equilibrium area composed by solid tristearin with a liquid phase and region 3 is the solid solution of both components.

Thermodynamic modeling of SLE data

The adjusted parameters obtained by three-suffix Margules and NRTL are presented in Table 9. One can observe that the root mean square deviation (RMSD) values for all the systems studied are low, which means that all models describe the experimental data in a good way, including the ideal assumption, which needs a smaller computational effort. Besides, in this thermodynamic study, the solid phase was considered ideal, and, for all the systems, including those that presented a solid solution in all the composition range, the models described very well the *liquidus* line.

$$\text{RMSD} = \sqrt{\sum_{i=1}^N \left(\frac{T_i^{\text{exp}} - T_i^{\text{cal}}}{N} \right)^2}$$

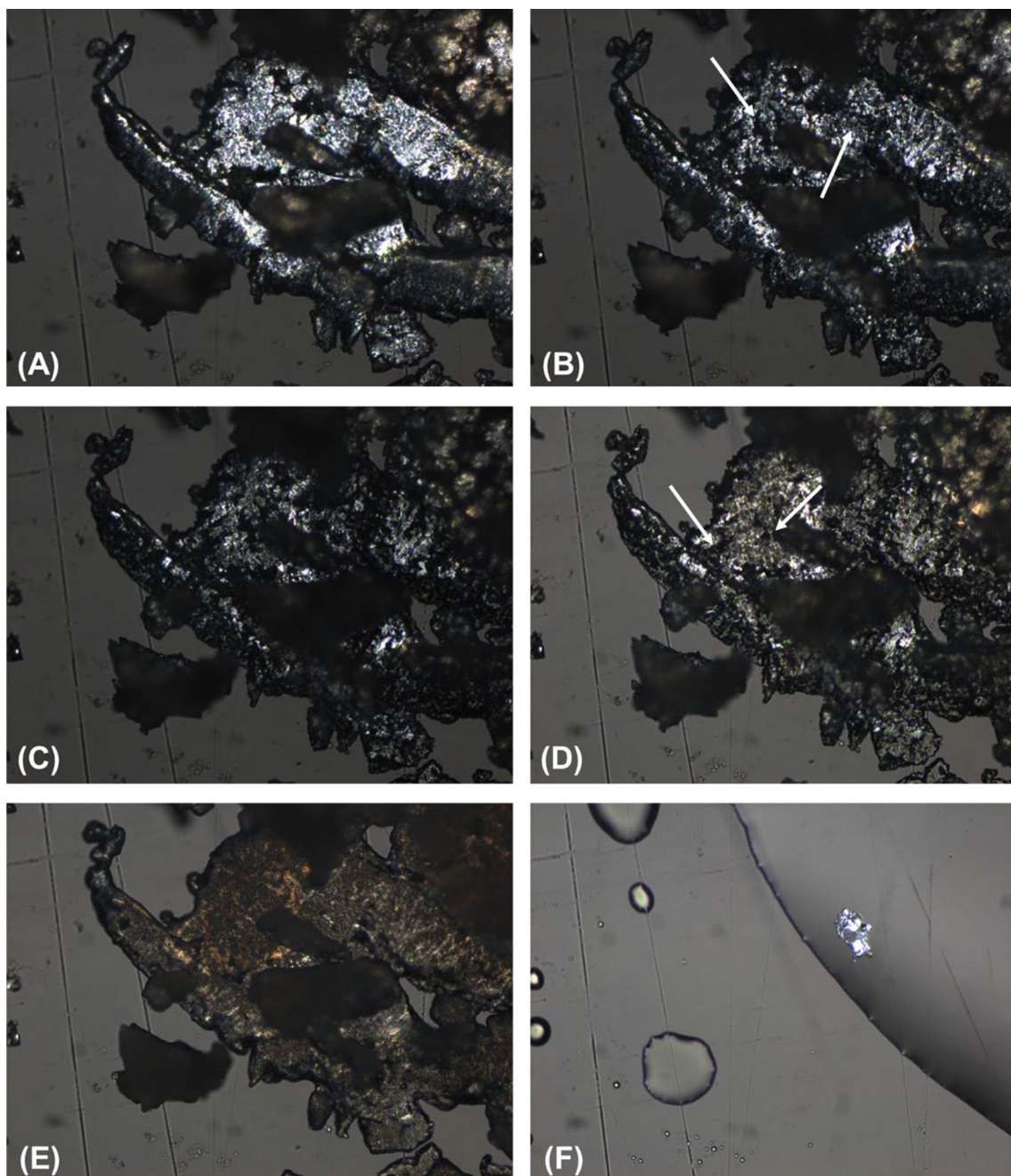


Fig. 10 Optical micrographs of the tristearin (1) + 1-tetradecanol (7) system at $x_1 = 0.1999$ with **A** 305.25 K; **B** 310.55 K; **C** 312.65 K; **D** 320.85 K; **E** 332.65 K; **F** 344.05 K. Magnification of 20 \times

Conclusion

The DSC technique was used to determine the phase diagram of the studied systems and it is considered an efficient and reliable method to study the SLE behavior of fatty mixtures. In this study, the melting temperature of pure tristearin was determined, and this property agrees very well with the data found in the literature. The study of the solid–liquid equilibrium (SLE) of fatty mixtures is

essential for the improvement and optimization of the processing of fatty based products. Due to the high complexity of the melting profile of fatty compounds and their mixtures, as tristearin + fatty acids and tristearin + fatty alcohol compounds, critical thermodynamic evaluation is important for process design and industrial quality requirements of products.

The phase diagrams of tristearin + fatty acids presented a monotectic behavior. Moreover, the tristearin (1) + lauric

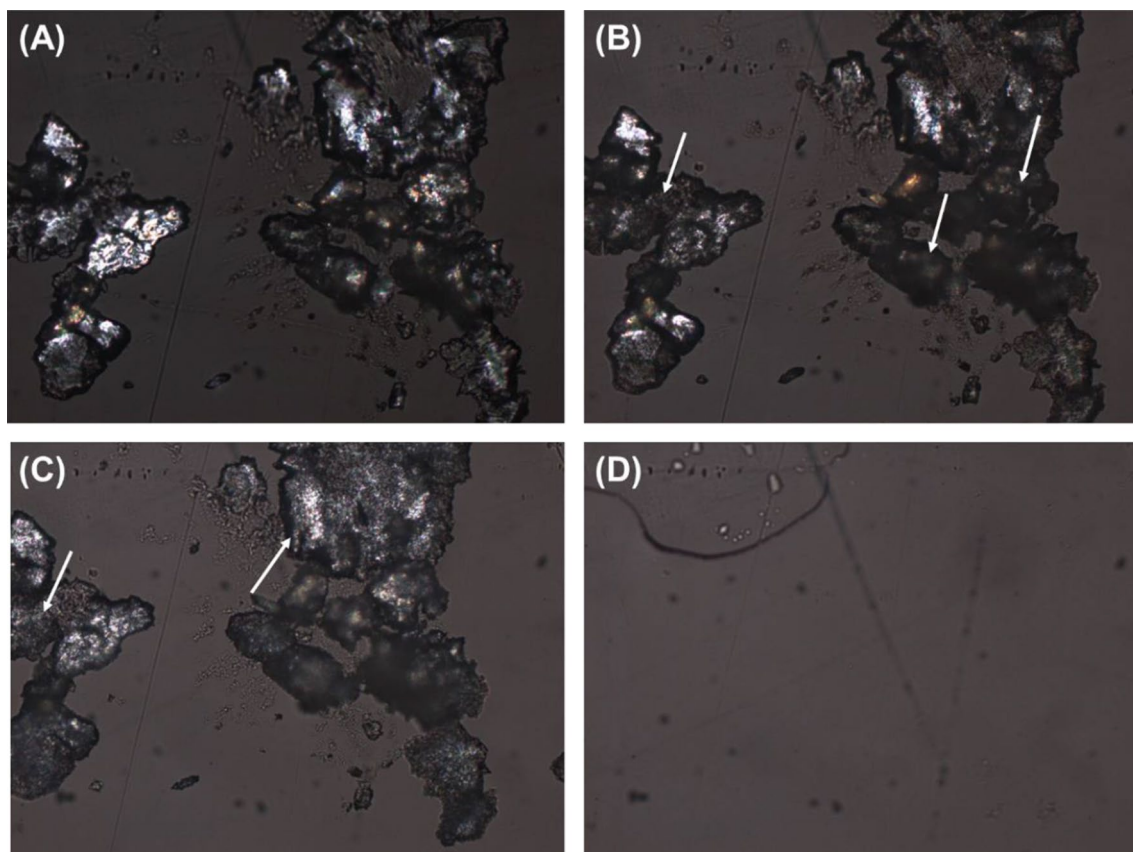


Fig. 11 Optical micrographs of the tristearin (1)+1-tetradecanol (7) system at $x_1=0.7997$ with **A** 305.15 K; **B** 316.35 K; **C**) 345.85 K; **D** 347.45 K. Magnification of 20 \times

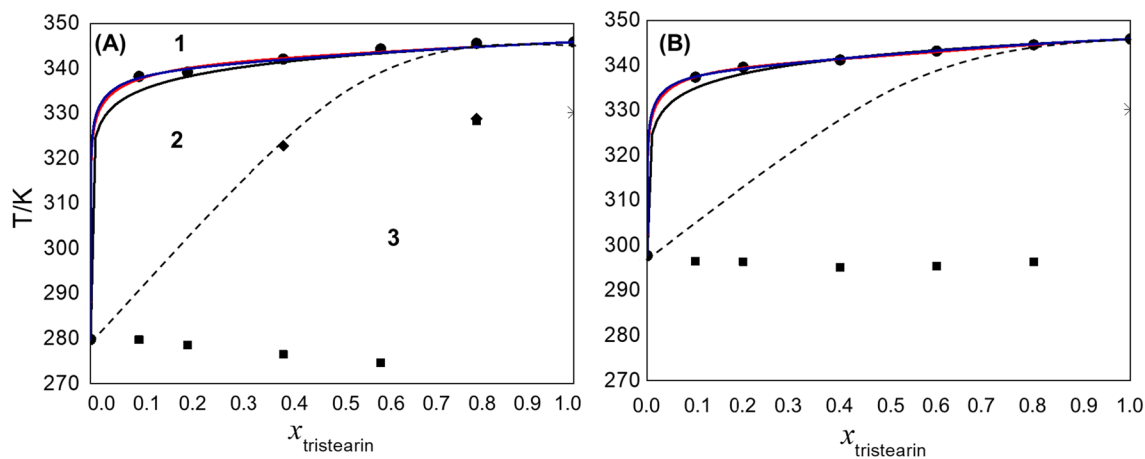


Fig. 12 SLE phase diagram of the **A** tristearin (1)+1-decanol (5) system; **B** tristearin (1)+1-dodecanol (6) binary system: (filled circle) melting temperature; (filled square) solid transition temperature; (filled diamond) exothermic transition temperature; (*) pure compo-

nent transition temperature; (black line) ideal model; (red line) three-suffix Margules; (blue line) NRTL; (dashed line) guide to the eyes of solid solution formation

acid (3) and tristearin (1) + myristic acid (4) systems presented a solid solution close to the pure triacylglycerol molar fraction, according to optical microscope images.

The systems formed by tristearin + fatty alcohol compounds seem to exhibit a solid solution formation in all the molar fraction composition range.

Table 9 Three-suffix Margules and NRTL adjusted parameters

Systems	Three-suffix Margules		NRTL ($\alpha_{12}=0.30$)		RMSD*		
	A_{ij} (J mol ⁻¹)	A_{ji} (J mol ⁻¹)	Δg_{ij} (J mol ⁻¹)	Δg_{ji} (J mol ⁻¹)	Three-suffix Margules	NRTL	Ideal
Tristearin (1) + capric acid (2)	1011.7330	1838.9685	3676.0776	-1430.0823	0.1165	0.1091	0.3103
Tristearin (1) + lauric acid (3)	166.9548	2401.7323	7145.3008	-2872.4968	0.5289	0.5223	0.3487
Tristearin (1) + myristic acid (4)	127.0978	1387.0495	5111.0434	-2654.4704	0.0810	0.1066	0.1721
Tristearin (1) + 1-decanol (5)	2188.4278	1135.3711	-2327.2022	5909.0658	0.5587	0.5234	0.5240
Tristearin (1) + 1-dodecanol (6)	2503.7680	-735.9480	-3242.3642	7869.6661	0.1101	0.1767	0.4050
Tristearin (1) + 1-tetradecanol (7)	2124.2343	151.4973	-2825.5039	6535.4144	0.1822	0.1248	0.3966
Average of RMSD					0.2629	0.2605	0.3594

All the six studied systems were modeled using the ideal assumption, three-suffix Margules, and NRTL models. All models were able to describe the *liquidus* line. However, the three-suffix Margules and NRTL models presented the best results, since they are more complex than ideal assumption. Thus, both models, three-suffix Margules can be considered thermodynamic.

Supplementary Information The online version contains supplementary material available at <https://doi.org/10.1007/s43153-022-00227-5>.

Author contributions PFP and MFC designed research; CMC, BEAC, MAJA conducted review, editing, and provided funding acquisition, project administration, and resources; PFP wrote the paper.

Funding The authors thank the Coordenação de Aperfeiçoamento de Pessoal de Nível Superior–Brazil (CAPES)–Finance Code 001, FAPESP (2014/21252-0 and 2018/19198-9), CNPq (305870/2014-9, 406963/2014-4, 306666/2020-0, 309780/2014-4, and 132149/2017-6), and FAEPEX/UNICAMP for the financial support. The authors also thank Espaço da Escrita–Pró-Reitoria de Pesquisa–UNICAMP–for the language services provided.

Availability of data and material The authors declare that the data and material are available.

Code availability Not applicable.

Declarations

Conflict of interest The authors declare no conflict of interest.

References

- Carareto NDD, Costa MC, Meirelles AJA, Pauly J (2015) High pressure solid-liquid equilibrium of fatty alcohols binary systems from 1-Dodecanol, 1-Tetradecanol, 1-Hexadecanol, and 1-Octadecanol. *J Chem Eng Data* 60:2966–2973
- Carareto NDD, Dos Santos AO, Rolemberg MP, Cardoso LP, Costa MC, Meirelles AJA (2014) ‘On the solid-liquid phase diagrams of binary mixtures of even saturated fatty alcohols: Systems exhibiting peritectic reaction’, *Thermochimica Acta*. Elsevier B.V., 589, pp 137–147. <https://doi.org/10.1016/j.tca.2014.05.022>.
- Costa MC, Rolemberg MP, Boros LAD, Krähenbühl MA, de Oliveira MG, Meirelles AJA (2007) Solid–liquid equilibrium of binary fatty acid mixtures. *J Chem Eng Data* 52:30–36. <https://doi.org/10.1021/je060146z>
- Costa MC, Rolemberg MP, Dos Santos AO, Cardoso LP, Krähenbühl MA, Meirelles AJA (2010) Solid-liquid equilibrium of tristearin with refined rice bran and palm oils. *J Chem Eng Data* 55:5078–5082. <https://doi.org/10.1021/je100647b>
- Costa MC, Boros LAD, Souza JA, Rolemberg MP, Krähenbühl MA, Meirelles AJA (2011) Solid–liquid equilibrium of binary mixtures containing fatty acids and triacylglycerols. *J Chem Eng Data* 56:3277–3284. <https://doi.org/10.1021/je200033b>
- Craven RJ, Lencki RW (2011) Binary phase behavior of diacid 1,3-diacylglycerols. *J Am Oil Chem Soc* 88:1125–1134. <https://doi.org/10.1007/s11746-011-1777-0>
- Da Silva RC, De Martini Soares FAS, Maruyama JM, Dagostinho NR, Silva YA, Ract JNR, Gioielli LA (2016) Microscopic approach of the crystallization of tripalmitin and tristearin by microscopy. *Chem Phys Lipid* 198:1–9. <https://doi.org/10.1016/j.chemphyslip.2016.04.004>
- de Matos FC, da Costa MC, Meirelles AJ, Batista EAC (2015) Binary solid-liquid equilibrium systems containing fatty acids, fatty alcohols and triolein by differential scanning calorimetry. *Fluid Phase Equilib* 404:1–8. <https://doi.org/10.1016/j.fluid.2015.06.015>
- de Matos FC, da Costa MC, Meirelles AJ, Batista EAC (2016) Binary solid-liquid equilibrium systems containing fatty acids, fatty alcohols and trilaurin by differential scanning calorimetry. *Fluid Phase Equilib* 423:74–83. <https://doi.org/10.1016/j.fluid.2016.04.008>
- Dorigheo Carareto ND, Costa MC, Meirelles AJA, Pauly J (2015) High pressure solid-liquid equilibrium of fatty alcohols binary systems from 1-DODECANOL, 1-Tetradecanol, 1-Hexadecanol, and 1-Octadecanol. *J Chem Eng Data* 60:2966–2973. <https://doi.org/10.1021/acs.jced.5b00330>
- Eckert KA, Dasgupta S, Selge B, Ay P (2016) Solid liquid phase diagrams of binary fatty acid mixtures—palmitic/stearic with oleic/linoleic/linolenic acid mixture. *Thermochim Acta* 630:50–63. <https://doi.org/10.1016/j.tca.2016.02.008>
- Fisk PR, Wildey RJ, Girling AE, Sanderson H, Belanger SE, Veenstra G, Nielsen A, Kasai Y, Willing A, Dyer SD, Stanton K (2009) Environmental properties of long chain alcohols. Part 1: physico-chemical, environmental fate and acute aquatic toxicity properties. *Ecotoxicol Environ Saf* 72:980–995. <https://doi.org/10.1016/j.ecoenv.2008.09.025>
- Garti N, Sato K (1988) Crystallization and polymorphism of fats and fatty acids. Marcel Dekker, Nova Iorque

- Höhne GWH, Hemminger WF, Flammerseim HJ (2003) Differential Scanning Calorimetry, 2nd edn. Springer, New York
- Humphrey KL, Narine SS (2005) Lipid phase behavior. In: Marangoni AG (ed) Fat crystal networks. Taylor & Francis, New York, p 854
- Inoue T, Hisatsugu Y, Ishikawa R, Suzuki M (2004a) Solid-liquid phase behavior of binary fatty acid mixtures: 2. Mixtures of oleic acid with lauric acid, myristic acid, and palmitic acid. *Chem Phys Lipid* 127:161–173. <https://doi.org/10.1016/j.chemphyslip.2003.10.013>
- Inoue T, Hisatsugu Y, Yamamoto R, Suzuki M (2004b) Solid-liquid phase behavior of binary fatty acid mixtures: 1. Oleic acid/stearic acid and oleic acid/behenic acid mixtures. *Chem Phys Lipid* 127:143–152. <https://doi.org/10.1016/j.chemphyslip.2003.09.014>
- Johnson RW (1988) Fatty alcohols. Fatty acids in industry. Marcel Dekker, New York, pp 217–231
- Kellens M, Reynaers H (1992) Study of the polymorphism of saturated monoacid triglycerides I: melting and crystallization behavior of tristearin. *Fat Sci Technol* 94:94–100. <https://doi.org/10.1002/lipi.19920940304>
- Kellens M, Meeussen W, Gehrke R, Reynaers H (1991) Synchrotron radiation investigations of the polymorphic transitions of saturated monoacid triglycerides. Part 1: Tripalmitin and tristearin. *Chem Phys Lipid* 58:131–144. [https://doi.org/10.1016/0009-3084\(91\)90119-V](https://doi.org/10.1016/0009-3084(91)90119-V)
- Kogan A, Garti N (2006) Microemulsions as transdermal drug delivery vehicles. *Adv Coll Interface Sci* 123–126:369–385. <https://doi.org/10.1016/j.cis.2006.05.014>
- Matovic M, Van Miltenburg JC, Los J, Gandolfo FG, Flöter E (2005) Thermal properties of tristearin by adiabatic and differential scanning calorimetry. *J Chem Eng Data* 50:1624–1630. <https://doi.org/10.1021/je050092d>
- Maximo GJ, Costa MC, Meirelles AJA (2013) Solid-liquid equilibrium of triolein with fatty alcohols. *Braz J Chem Eng* 30:33–43. <https://doi.org/10.1590/S0104-66322013000100005>
- Maximo GJ, Carareto NDD, Costa MC, dos Santos AO, Cardoso LP, Krähenbühl MA, Meirelles AJA (2014a) On the solid-liquid equilibrium of binary mixtures of fatty alcohols and fatty acids. *Fluid Phase Equilib* 366:88–98. <https://doi.org/10.1016/j.fluid.2014.01.004>
- Maximo GJ, Costa MC, Meirelles AJA (2014b) The Crystal-T algorithm: a new approach to calculate the SLE of lipidic mixtures presenting solid solutions. *Phys Chem Chem Phys* 16:16740–16754. <https://doi.org/10.1039/c4cp01529k>
- Maximo GJ, Carareto NDD, Costa MC (2019) Solid-Liquid Equilibrium in Food Processes. In: Thermodynamics of Phase Equilibria in Food Engineering. 1st edn. Academic Press, Cambridge, p 684
- Oh JH, McCurdy AR, Clark S, Swanson BG (2002) Characterization and thermal stability of polymorphic forms of synthesized tristearin. *J Food Sci* 67:911–2917. <https://doi.org/10.1111/j.1365-2621.2002.tb08837.x>
- Pelaquim FP, Cardoso de Matos F, Cardoso LP, Caldas Batista EA, de Almeida J, Meirelles A, Conceição da Costa M (2019) Solid-liquid phase equilibrium diagrams of binary mixtures containing fatty acids, fatty alcohol compounds and tripalmitin using differential scanning calorimetry. *Fluid Phase Equilib* 497:19–32. <https://doi.org/10.1016/j.fluid.2019.05.020>
- Pernetti M, van Malssen KF, Flöter E, Bot A (2007) Structuring of edible oils by alternatives to crystalline fat. *Curr Opin Colloid Interface Sci* 12:221–231. <https://doi.org/10.1016/j.cocis.2007.07.002>
- Persson M (2008) Alpha stable fats. *Lipid Technol* 20:13–16. <https://doi.org/10.1002/lite.200700099>
- Prausnitz JM, Lichtenthaler RN, de Azevedo EG (1999) Molecular thermodynamics of fluid-phase equilibria. 3rd edn, Nopardazan. Prentice Hall, Nova Jersey. [https://doi.org/10.1016/0021-9614\(70\)90078-9](https://doi.org/10.1016/0021-9614(70)90078-9)
- Singh SK, Jalali AF, Aldén M (1999) Modulated temperature differential scanning calorimetry for examination of tristearin polymorphism: 2. Isothermal Crystallization of Metastable Forms. *J Am Oil Chem Soc* 76:507–510. <https://doi.org/10.1007/s11746-999-0031-5>
- Tadie M, Bahadur I, Reddy P, Ngema PT, Naidoo P, Deenadayalu N, Ramjugernath D (2013) Solid-liquid equilibria measurements for binary systems comprising (butyric acid + propionic or pentanoic acid) and (heptanoic acid + propionic or butyric or pentanoic or hexanoic acid). *J Chem Thermodyn* 57:485–492. <https://doi.org/10.1016/j.jct.2012.09.019>
- Timms RE (1984) Phase behaviour of fats and their mixtures. *Prog Lipid Res* 23:1–38. [https://doi.org/10.1016/0163-7827\(84\)90004-3](https://doi.org/10.1016/0163-7827(84)90004-3)
- Vetterling WT, Teukolsky SA, Press WH, Flannery BP (1992) Numerical Recipes in F77. 2nd edn, Numerical Methods for Fortran 77: the art of scientific computing. 2nd edn. Press Syndicate of the University of Cambridge. <http://www.papers3://publication/uuid/42C52282-20B5-4159-9E1B-2E89F2631AAA>
- Webster GR, Bisset NB, Cahill DM, Jones P, Killick A, Hawley A, Boyd BJ (2018) Tristearin as a model cuticle for high-throughput screening of agricultural adjuvant systems. *ACS Omega* 3:16672–16680. <https://doi.org/10.1021/acsomega.8b02656>
- Wei D, Han S, Wang B (2014) Solid-liquid phase equilibrium study of binary mixtures of n-octadecane with capric, and lauric acid as phase change materials (PCMs). *Fluid Phase Equilib* 373:84–88. <https://doi.org/10.1016/j.fluid.2014.04.020>
- Wesdorp LH (1990) Liquid-Multiple solid phase equilibria in fats. Universidade de Tecnologia de Delft
- Wright AJ, Marangoni AG (2005) Physical Properties of Fats and Oils. Handbook of Functional Lipids. CRC Press, Florida, pp 135–162
- Yui K, Itsukaichi Y, Kobayashi T, Tsuji T, Fukui K, Maeda K, Kuramochi H (2017) Solid-liquid equilibria in the binary systems of saturated fatty acids or triglycerides (C12 to C18) + hexadecane. *J Chem Eng Data* 62:35–43. <https://doi.org/10.1021/acs.jced.6b00355>
- Zhang Z, Yuan Y, Zhang N, Cao X (2015) Thermophysical Properties of Some Fatty Acids/Surfactants as Phase Change Slurries for Thermal Energy Storage. *J Chem Eng Data* 60:2495–2501. <https://doi.org/10.1021/acs.jced.5b00371>
- Zhao P, Yue Q, He H, Gao B, Wang Y, Li Q (2014) Study on phase diagram of fatty acids mixtures to determine eutectic temperatures and the corresponding mixing proportions. *Appl Energy* 115:483–490. <https://doi.org/10.1016/j.apenergy.2013.10.048>

Publisher's Note Springer Nature remains neutral with regard to jurisdictional claims in published maps and institutional affiliations.

Authors and Affiliations

Fernanda Paludetto Pelaquim¹ · Flávio Cardoso de Matos² · Eduardo Augusto Caldas Batista² · Antonio José de Almeida Meirelles² · Mariana Conceição da Costa¹ 

✉ Mariana Conceição da Costa
mcosta@feq.unicamp.br

¹ School of Chemical Engineering, University of Campinas, UNICAMP, 500 Albert Einstein Avenue, Campinas zip code 13083-852, SP, Brazil

² School of Food Engineering, University of Campinas, UNICAMP, 500 Albert Einstein Avenue, Campinas zip code 13083-852, SP, Brazil